Reference hypernetted chain theory for ferrofluid bilayer: Distribution functions compared with Monte Carlo

Evgeny A. Polyakov and Pavel N. Vorontsov-Velyaminov

Citation: The Journal of Chemical Physics **141**, 084109 (2014); doi: 10.1063/1.4894135
View online: http://dx.doi.org/10.1063/1.4894135
View Table of Contents: http://scitation.aip.org/content/aip/journal/jcp/141/8?ver=pdfcov
Published by the AIP Publishing

Reference hypernetted chain theory for ferrofluid bilayer: Distribution functions compared with Monte Carlo

Evgeny A. Polyakov[a] and Pavel N. Vorontsov-Velyaminov[b]
Faculty of Physics, St. Petersburg State University, 198504 St. Petersburg, Russia

(Received 18 July 2014; accepted 17 August 2014; published online 29 August 2014)

Properties of ferrofluid bilayer (modeled as a system of two planar layers separated by a distance h and each layer carrying a soft sphere dipolar liquid) are calculated in the framework of inhomogeneous Ornstein-Zernike equations with reference hypernetted chain closure (RHNC). The bridge functions are taken from a soft sphere ($1/r^{12}$) reference system in the pressure-consistent closure approximation. In order to make the RHNC problem tractable, the angular dependence of the correlation functions is expanded into special orthogonal polynomials according to Lado. The resulting equations are solved using the Newton-GRMES algorithm as implemented in the public-domain solver NITSOL. Orientational densities and pair distribution functions of dipoles are compared with Monte Carlo simulation results. A numerical algorithm for the Fourier-Hankel transform of any positive integer order on a uniform grid is presented. © *2014 AIP Publishing LLC*. [http://dx.doi.org/10.1063/1.4894135]

I. INTRODUCTION

The inhomogeneous Ornstein-Zernike (OZ) equations with reference hypernetted chain closure (RHNC) closure[1,2] is, to the authors' knowledge, one of the most accurate theories to calculate the properties of inhomogeneous liquids on the level of pair correlations. In particular, in the field of confined liquids it has been successfully applied to the model of Lennard-Jones particles in a narrow slit between two walls with the Steele wall-particle potential.[1] The theoretical density profiles and wall pressures are in excellent agreement with simulations.[1] Another application of RHNC is for electric double layers in mono- and divalent electrolytes modeled as uniformly charged planes with charged point particles between them, where the theory correctly predicts interactions and ion distribution functions.[2–4] The theory[5] was used to illustrate the mechanisms behind such phenomena as charge inversion and overcompensation of the surface charge.

In the field of quasi-two-dimensional ferrofluids, the RHNC was applied to the ferrofluid monolayer model where the hard sphere particles carrying three-dimensional magnetic dipoles are constrained to a planar surface, and an external field is acting perpendicular to the plane.[6] Theoretical angular distribution functions and projections of the pair distribution functions on the standard rotational invariants agree with Monte Carlo (MC) simulations.

The current situation provides an interesting opportunity to combine the aforementioned RHNC theories. The system of two parallel planar walls, each wall carrying a two-dimensional dipolar fluid, with charged particles between them can serve as a rough model to investigate the role of electrostatic interactions in quite a different system, e.g., interaction between lipid membranes with dipolar approximation of headgroups[7–13] or clay platelets,[14,15] etc. As a first step in this direction we present in this work RHNC calculations for the model of symmetric ferrofluid bilayer. It is a system of two planar layers separated by a distance h and each layer is carrying a soft sphere dipolar liquid of dipole moment μ. This system itself can serve as a crude model of interactions between layers in magnetic films,[16–18] or the aforementioned systems of lipid membranes and clay platelets. Moreover, not long ago a Monte Carlo study of such a system (with hard spheres instead of soft ones) was carried out[19] and we are unaware of the corresponding theoretical treatment by integral equations. There is HNC calculation for bilayer of dipoles with their direction fixed perpendicularly to the bilayer's plane,[14] and a series of works on bilayer with orientable dipoles but treated within perturbation theory.[20–22]

In this work, the angular distribution functions and pair correlations for a model of ferrofluid bilayer are calculated and compared with Monte Carlo simulation. A number of methodological issues are considered. The dipole-dipole pair correlation functions in this system are five-dimensional, taking into account circular symmetry. In order to make the RHNC problem tractable, the angular dependence of the correlation functions is expanded into special polynomials according to Lado.[23,24] These polynomials are constructed to be orthogonal with respect to one-body orientational distribution function $f(\cos\theta)$. In order to speed up the solution of integral equations we employ Newton-GRMES algorithm[25] as implemented in the public-domain solver NITSOL.[26] This algorithm solves a system of nonlinear algebraic equations $F(x) = 0$ where $F(x)$ is a vector function in a space of dimension n ($F : \mathrm{R}^n \to \mathrm{R}^n$). In our case $F(x)$ is formed from differences in distribution functions between successive iterations of RHNC equations. Finally, since the symmetry of bilayer pair functions is lower than that of monolayer ones, we have to compute the Hankel transforms of even and odd orders on a common grid. To address this issue, a numerical algorithm

[a]Electronic mail: e.a.polyakov@gmail.com
[b]Electronic mail: voron.wgroup@gmail.com

for the Fourier-Hankel transform of any positive integer order on uniform grid is presented.

In Sec. II, we describe the bilayer model and extend the integral equations of Ref. 6 to the bilayer case. In Sec. III, we describe our Monte Carlo simulations. Section IV is devoted to the comparison of RHNC and Monte Carlo results and a conclusion is made. In Appendix A, we describe our approach to the numerical Fourier-Hankel transform and in Appendix B we summarize the numerical procedure of the solution of RHNC equations.

II. INTEGRAL EQUATION FORMULATION

The system consists of particles with permanent point dipole moment μ interacting via soft sphere and dipolar potentials. The particle positions are constrained to one of the two planar layers (hereinafter denoted as b (bottom) and t (top)), separated by a distance h. The particles are distributed in each layer with a uniform average surface number density ρ. They are allowed to move along the layers they belong to, and the dipole moments can orient in full 3D space. No exchange of particles between layers b and t is allowed. The interaction potential between the particles is pairwise additive and is presented as[27]

$$u\left(\boldsymbol{r}_{ij}, \hat{\boldsymbol{\mu}}_i, \hat{\boldsymbol{\mu}}_j\right) = 4\lambda\left(\frac{d}{r_{ij}}\right)^{12} - \left(\frac{1}{r_{ij}}\right)^{3}\mu^2 \times [3(\hat{\boldsymbol{\mu}}_i\cdot\hat{\boldsymbol{r}}_{ij})(\hat{\boldsymbol{\mu}}_j\cdot\hat{\boldsymbol{r}}_{ij}) - \hat{\boldsymbol{\mu}}_i\cdot\hat{\boldsymbol{\mu}}_j], \quad (1)$$

where $\hat{\boldsymbol{\mu}}_i$ is the unit direction vector of the dipole moment of the particle i, $\hat{\boldsymbol{r}}_{ij} = \boldsymbol{r}_{ij}/r_{ij}$ is the unit direction vector from particle j to i, λ is the energy scale, and d is the length scale. Reduced units $\rho^\star = \rho d^2$ for surface density, $\mu^\star = \mu/\sqrt{d^3\lambda}$ for dipole moment, $s^\star = s/d$ for length and $\beta^\star = \beta\lambda$ for inverse temperature are used throughout the paper. In further relations the stars are omitted. Due to the lateral translational and circular symmetry of the system we split the radius vector $\boldsymbol{r}_{ij}$ as

$$\boldsymbol{r}_{ij} = \boldsymbol{s}_{ij} + z_{ij}\hat{\boldsymbol{e}}_z, \quad (2)$$

where $\hat{\boldsymbol{e}}_z$ is the unit vector perpendicular to the layers (directed from b to t) and z_{ij} can have values 0, $+h$, $-h$ depending on what layer the particles i and j belong to.

The hamiltonian of the model (1) possesses the vertical (transverse) reflection symmetry. However, the corresponding thermodynamic state can break this symmetry. Since currently there is no clear evidence for such symmetry breaking in thin films,[19,28] and we are mainly interested in extension of this model to colloids, we will look only for symmetrical solutions of the integral equations. This will allow us to reduce by half the number of the unknowns. So we map the bilayer onto a monolayer system of two components (b and t) with identical thermodynamical properties. We define the interaction potential (1) between the particles of the same component as

$$u_{bb}(\boldsymbol{s}_{ij}, \hat{\boldsymbol{\mu}}_i, \hat{\boldsymbol{\mu}}_j) = u_{tt}(\boldsymbol{s}_{ij}, \hat{\boldsymbol{\mu}}_i, \hat{\boldsymbol{\mu}}_j) = 4\left(\frac{1}{s_{ij}}\right)^{12} - \left(\frac{1}{s_{ij}}\right)^{3}\mu^2 \times [3(\hat{\boldsymbol{\mu}}_i\cdot\hat{\boldsymbol{s}}_{ij})(\hat{\boldsymbol{\mu}}_j\cdot\hat{\boldsymbol{s}}_{ij}) - \hat{\boldsymbol{\mu}}_i\cdot\hat{\boldsymbol{\mu}}_j] \quad (3)$$

and between the particles of different components as

$$u_{bt}(\boldsymbol{s}_{ij}, \hat{\boldsymbol{\mu}}_i, \hat{\boldsymbol{\mu}}_j) = 4\left(\frac{1}{s_{ij}^2+h^2}\right)^{6} - \left(\frac{1}{s_{ij}^2+h^2}\right)^{5/2}\mu^2 \times [3(\hat{\boldsymbol{\mu}}_i\cdot[\boldsymbol{s}_{ij}+h\hat{\boldsymbol{e}}_z]) \times (S\hat{\boldsymbol{\mu}}_j\cdot[\boldsymbol{s}_{ij}+h\hat{\boldsymbol{e}}_z]) - \hat{\boldsymbol{\mu}}_i\cdot S\hat{\boldsymbol{\mu}}_j], \quad (4)$$

where we have introduced the reflection symmetry operation S: $S\hat{\boldsymbol{\mu}}_j$ is the vector $\hat{\boldsymbol{\mu}}_j$ but with inverted sign of its z-component; thus we take into account the fact that b- and t-components face each other from the opposite directions but otherwise are indistinguishable.

The one-body density at each layer is defined as

$$\rho^{(1)}(\boldsymbol{s},\omega) = \left\langle\sum_j \delta(\boldsymbol{s}-\boldsymbol{s}_j)\delta\left(\omega-\omega_j\right)\right\rangle = \frac{\rho}{4\pi}f(\omega), \quad (5)$$

where $\omega = (\theta, \phi)$ are spherical angles of the dipole moment and the orientational distribution function of dipoles $f(\omega)$ is one of the unknowns of the integral equations. Due to the lateral translational and circular symmetry, f depends only on zenith angle θ of the dipole moment with respect to zenith direction $\hat{\boldsymbol{e}}_z$, $f(\omega) = f(\cos\theta)$. The intralayer two-body density

$$\rho_{bb}^{(2)}(\boldsymbol{s},\omega,\boldsymbol{s}',\omega') = \rho_{tt}^{(2)}(\boldsymbol{s},\omega,\boldsymbol{s}',\omega') = \left\langle\sum_{\substack{i,\,j\in b\\ i\neq j}}\delta(\boldsymbol{s}-\boldsymbol{s}_i)\delta(\omega-\omega_i) \times\ \delta(\boldsymbol{s}'-\boldsymbol{s}_j)\delta(\omega'-\omega_j)\right\rangle = \frac{\rho^2}{(4\pi)^2}f(\omega)f(\omega') \times g_{bb}(\boldsymbol{s}-\boldsymbol{s}',\omega,\omega') \quad (6)$$

defines the intralayer generalized distribution function $g_{bb}(12) = g_{tt}(12) = g_{bb}(\boldsymbol{s}_{12},\omega_1,\omega_2)$ between the particles

of the same component. The interlayer two-body density

$$\rho_{bt}^{(2)}(\boldsymbol{s},\omega,\boldsymbol{s}',\omega') = \rho_{tb}^{(2)}(\boldsymbol{s}',\omega',\boldsymbol{s},\omega) = \left\langle \sum_{i\in b}\delta(\boldsymbol{s}-\boldsymbol{s}_i)\delta(\omega-\omega_i) \times \sum_{j\in t}\delta(\boldsymbol{s}'-\boldsymbol{s}_j)\delta(\omega'-\omega_j)\right\rangle = \frac{\rho^2}{(4\pi)^2} f(\omega) f(\omega') \times g_{bt}(\boldsymbol{s}-\boldsymbol{s}',\omega,\omega') \quad (7)$$

defines the interlayer generalized distribution function $g_{bt}(12) = g_{tb}(21) = g_{bt}(\boldsymbol{s}_{12},\omega_1,\omega_2)$ between particles of different components.

The functions $f(\cos\theta)$, $g_{bb}(12)$, and $g_{bt}(12)$ represent the list of the quantities to be found from the integral equations. To determine them we follow the work of Lomba, Lado *et al.*[6] and generalize the theory to the bilayer case. The first Kirkwood-Born-Green-Yvon (KBGY) equation,

$$\frac{d}{dx}\ln[f(x)] = -\frac{\beta\rho}{4\pi}\int d\boldsymbol{s}\, d\omega' f(\omega') g_{bb}(\boldsymbol{s},\omega,\omega') \times \frac{d}{dx}u_{bb}(\boldsymbol{s},\omega,\omega') - \frac{\beta\rho}{4\pi}\int d\boldsymbol{s}\, d\omega' f(\omega') g_{bt}(\boldsymbol{s},\omega,\omega') \times \frac{d}{dx}u_{bt}(\boldsymbol{s},\omega,\omega'), \quad (8)$$

couples one-body to two-body distributions; here (and below) $x = \cos\theta = \omega_z$. The inhomogeneous OZ equations

$$h_{\mu\nu}(\boldsymbol{s}_{12},\omega_1,\omega_2) = c_{\mu\nu}(\boldsymbol{s}_{12},\omega_1,\omega_2) + \frac{\rho}{4\pi}\sum_{\eta}\int d\boldsymbol{s}_3\, d\omega_3 f(x_3) \times h_{\mu\eta}(\boldsymbol{s}_{13},\omega_1,\omega_3) c_{\eta\nu}(\boldsymbol{s}_{32},\omega_3,\omega_2) \quad (9)$$

represent exact relations between the generalized total correlation functions $h_{\mu\nu} = g_{\mu\nu} - 1$ and the generalized direct correlation functions $c_{\mu\nu}$. Here greek letters denote the component (b or t). Since OZ equation introduces additional unknown variables $c_{\mu\nu}$, in order to make the system complete we need a closure, i.e., a relation between $h_{\mu\nu}$ and $c_{\mu\nu}$. In HNC family of theories, this is[29]

$$c_{\mu\nu}(\boldsymbol{s},\omega_1,\omega_2) = \exp[-\beta u_{\mu\nu}(\boldsymbol{s},\omega_1,\omega_2) + \gamma_{\mu\nu}(\boldsymbol{s},\omega_1,\omega_2) + b_{\mu\nu}(\boldsymbol{s},\omega_1,\omega_2)] - 1 - \gamma_{\mu\nu}(\boldsymbol{s},\omega_1,\omega_2), \quad (10)$$

where the indirect correlation function $\gamma_{\mu\nu} = h_{\mu\nu} - c_{\mu\nu}$. The relation (10) is exact. However, the bridge function $b_{\mu\nu}(\boldsymbol{s},\omega_1,\omega_2)$ is not known in any efficiently computable form. It is the computational recipe for $b_{\mu\nu}(\boldsymbol{s},\omega_1,\omega_2)$ where the approximation comes. In HNC, one simply sets $b_{\mu\nu} = 0$. However, according to the RHNC procedure we select a reference system: particles interacting with the soft sphere potential

$$u^{\mathrm{ref}}(\boldsymbol{s}_{ij}) = 4\lambda^{\mathrm{ref}}\left(\frac{1}{s_{ij}}\right)^{12}, \quad (11)$$

with the same geometry and at the same surface density ρ as the full system. Then we determine the indirect correlation function $\gamma_{\mu\nu}^{\mathrm{ref}}$ of the reference system by solving the homogeneous variant of OZ equation (9) and the pressure-consistent (PC) closure[30–32] (also called the Rowlinson-Lado closure[33]),

$$c_{\mu\nu}^{\mathrm{ref}}(\boldsymbol{s}) = h_{\mu\nu}^{\mathrm{ref}}(\boldsymbol{s}) - (1-\xi)\left[g_{\mu\nu}^{\mathrm{ref}}(\boldsymbol{s})\, e^{\beta u_{\mu\nu}^{\mathrm{ref}}(\boldsymbol{s})} - 1\right] - \xi\ln\left[g_{\mu\nu}^{\mathrm{ref}}(\boldsymbol{s})\, e^{\beta u_{\mu\nu}^{\mathrm{ref}}(\boldsymbol{s})}\right], \quad (12)$$

where the two-component version $u_{\mu\nu}^{\mathrm{ref}}$ of u^{ref} is constructed similar to (3) and (4). The parameter ξ is chosen to achieve consistency of the virial p_v and compressibility pressures p_c,[30–32] where for our case

$$p_v = 2\beta^{-1}\rho - \frac{1}{2}\rho^2\int g_{bb}^{\mathrm{ref}}(s)\, s\frac{\partial u_{bb}^{\mathrm{ref}}}{\partial s}(s)\, 2\pi s\, ds - \frac{1}{2}\rho^2\int g_{bt}^{\mathrm{ref}}(s)\, s\frac{\partial u_{bt}^{\mathrm{ref}}}{\partial s}(s)\, 2\pi s\, ds, \quad (13)$$

$$\frac{\partial p_c}{\partial\rho} = 2\beta^{-1}\left\{1 - \rho\int\left[c_{bb}^{\mathrm{ref}}(s) + c_{bt}^{\mathrm{ref}}(s)\right]2\pi s\, ds\right\}. \quad (14)$$

The bridge function is approximated as[33]

$$b_{\mu\nu}(\boldsymbol{s},\omega_1,\omega_2) \approx (1-\xi)\left\{\ln\left[g_{\mu\nu}^{\mathrm{ref}}(\boldsymbol{s})\, e^{\beta u_{\mu\nu}^{\mathrm{ref}}(\boldsymbol{s})}\right] - g_{\mu\nu}^{\mathrm{ref}}(\boldsymbol{s})\, e^{\beta u_{\mu\nu}^{\mathrm{ref}}(\boldsymbol{s})} + 1\right\}. \quad (15)$$

The value of the reference potential parameter λ^{ref} was chosen as $\lambda^{\mathrm{ref}} = 1.0$.

Equations (8)–(15) now form a closed set. Then we should transform them into a form suitable for numerical computation. We expand the angular dependence of pair functions into the generalized spherical harmonics,[23]

$$\mathcal{Y}_{lm}(\omega) = \frac{1}{\sqrt{4\pi}}(-1)^m e^{im\phi}\mathcal{P}_{lm}(\cos\theta), \quad (16)$$

which are constructed to be orthogonal with respect to the weight $f(\omega)$,

$$\int d\omega\, f(\omega)\,\mathcal{Y}_{lm}(\omega)\,\mathcal{Y}_{l'm'}^{*}(\omega) = \delta_{ll'}\delta_{mm'}. \quad (17)$$

The reader is referred to Refs. 23 and 24 for additional information on the computational procedure. Here we note for completeness that the generalized Legendre polynomials $\mathcal{P}_{lm}(x)$ are defined as

$$\mathcal{P}_{lm}(x) = \frac{(\mathrm{sgn}\,\bar{m})^m}{\mathcal{N}_{lm}}(1-x^2)^{|m|/2}\mathcal{Q}_{l-|m|}^{|m|}(x), \quad (18)$$

where $\overline{m} = -m$ and $\mathcal{Q}_l^m(x)$ are monic polynomials of the order l. The $\mathcal{Q}_l^m(x)$ are constructed to be orthogonal with

respect to the weight $f(x)(1-x^2)^m$,

$$\frac{1}{2}\int_{-1}^{1} dx\, f(x)(1-x^2)^m \mathcal{Q}_{l_1}^m(x)\mathcal{Q}_{l_2}^m(x) = \delta_{l_1 l_2}\mathcal{N}_{lm}^2, \qquad (19)$$

where $\mathcal{N}_{lm}$ is their normalization factor. The orthogonality is achieved by defining them through the recursion relation

$$\mathcal{Q}_{l+1}^m(x) = (x-a_l)\mathcal{Q}_l^m(x) - b_l\mathcal{Q}_{l-1}^m(x) \qquad (20)$$

and the coefficients a_l, b_l of the recursion relation are calculated by Press and Teukolsky algorithm.[34,35] This algorithm requires the $f(x)$ to be defined on a grid of a fine Gaussian quadrature rule. In this paper, we call this quadrature rule the "reference" quadrature since it is fixed throughout the calculation. We use the Gauss-Legendre reference quadrature in $[-1, 1]$ with 128 grid points as the reference quadrature. Since it is used only to store one-dimensional array of $f(x)$ values, the dependence on the reference grid size is not memory intensive. However, the correlation functions are four-dimensional in angular variables and the memory requirements become prohibitive rather quickly. In order to cope with this the generalized spherical harmonics expansion is truncated at the order $l_{\max}$; here we use $l_{\max} = 3$. Then an $(l_{\max}+1)$-point Gaussian quadrature on x variable is constructed for the weight $f(x)$. We call this quadrature "adaptive" since it is recalculated for each new estimate of $f(x)$. The dependence on zenith angle of the pair functions is discretized on the nodes of this quadrature. Due to the fundamental theorem of Gaussian quadratures the orthogonality relations (19) are exactly reproduced on the adaptive grid for $m \le l_{\max}$ and $l_1,\ l_2 \le l_{\max} - m$. The dependence on azimuth ϕ is uniformly discretized in $[0, 2\pi)$ with the minimum number of points $2(l_{\max}+1)$ in order to avoid the Nyquist aliasing phenomena. This grid is fixed throughout the calculation. Note that in this work we use the smallest quadratures which are able to reproduce the orthogonality relations between the retained generalized spherical harmonics. In our case this proved to be enough to accurately sample the closure (10). However according to the paper[36] in general it may be necessary to increase the number of points of the quadratures since the nonlinearity of (10) widens its angular spectrum.

The pair functions are expanded into the generalized spherical harmonics as

$$\gamma_{\mu\nu}(\boldsymbol{s},\omega_1,\omega_2) = 4\pi \sum_{l_1,l_2,m_1,m_2} \gamma_{\mu\nu}(s;l_1m_1l_2m_2) \times \mathcal{Y}_{l_1m_1}(\omega_1)\mathcal{Y}_{l_2\overline{m}_2}(\omega_2) \times \exp[-i(m_1-m_2)\phi_s], \qquad (21)$$

where ϕ_s is the azimuthal angle of the planar vector $\boldsymbol{s}$ with respect to the x-axis. The dependence on ϕ_s is necessary when deriving symmetry properties of the expansion and the Fourier transform relations. However in practical calculations we always choose $\phi_s = 0$. Note that in case of monolayer systems the pair functions are symmetric with respect to the inversion of the connecting vector $\boldsymbol{r}_{ij}$.[6] This leads to the selection rule for the coefficients in (21): they are non-zero only if $m_1 - m_2$ is an even number.[6] However, when we turn to the bilayer case the symmetry is lost, and all values of m_1, m_2 are allowed. It can also be shown by performing the generalized spherical expansion of the pair potential (4): it contains the terms such as $\mathcal{Y}_{11}(\omega_1)\mathcal{Y}_{10}(\omega_2)$ and $\mathcal{Y}_{1\bar{1}}(\omega_1)\mathcal{Y}_{10}(\omega_2)$.

The generalized spherical expansion coefficients are calculated as

$$\gamma_{\mu\nu}(s;l_1m_1l_2m_2) = \frac{1}{4\pi}\int_0^{2\pi}\phi_1\int_0^{2\pi}\phi_2\int_{-1}^{1}dx_1\int_{-1}^{1}dx_2 \times f(x_1)f(x_2)\gamma_{\mu\nu}(s,x_1,x_2,\phi_1,\phi_2) \times \mathcal{Y}^*_{l_1m_1}(\omega_1)\mathcal{Y}^*_{l_2m_2}(\omega_2), \qquad (22)$$

where the fourfold integral is evaluated using the adaptive Gaussian quadrature described above (see Appendix B for explicit expressions). Equation (22) should be applied for expansion of the closure (10) with care, in order not to lose the numerical accuracy. We refer the reader to the paper[36] for comprehensive analysis of this point.

To transform the OZ equation (9) into numerically tractable form, the convolution in the lateral variables should be eliminated. We accomplish this by using the two-dimensional Fourier transform

$$\tilde{\gamma}_{\mu\nu}(12) = \int d\boldsymbol{s}\,\gamma_{\mu\nu}(12)\,e^{i\boldsymbol{k}\cdot\boldsymbol{s}}. \qquad (23)$$

The expansion coefficients of a pair function are related to their Fourier transforms through Hankel transforms[6]

$$\tilde{\gamma}_{\mu\nu}(k;l_1m_1l_2m_2) = 2\pi i^{|m_1-m_2|}\int_0^\infty dr\,r \times \gamma_{\mu\nu}(s;l_1m_1l_2m_2) \times J_{|m_1-m_2|}(ks), \qquad (24)$$

$$\gamma_{\mu\nu}(s;l_1m_1l_2m_2) = \frac{1}{2\pi i^{|m_1-m_2|}}\int_0^\infty dk\,k \times \tilde{\gamma}_{\mu\nu}(k;l_1m_1l_2m_2) \times J_{|m_1-m_2|}(ks), \qquad (25)$$

where $J_m(x)$ is the Bessel function of the order m. For the numerical calculation of the Hankel transforms the s-dependence of pair functions is uniformly discretized in $[0,\ s_{\max}]$ with $s_{\max} = 12$ and with 1000 discretization points being used. The discretization in s-space corresponds to the conjugate discretization in k-space and the action of the Hankel transform of the order $|m_1 - m_2|$ is represented as a matrix operation

$$\tilde{\gamma}_{\mu\nu}(k_j;l_1m_1l_2m_2) = \sum_i B_{|m_1-m_2|}(s\to k)_{ji} \times \gamma_{\mu\nu}(s_i;l_1m_1l_2m_2), \qquad (26)$$

$$\gamma_{\mu\nu}(s_j;l_1m_1l_2m_2) = \sum_i B_{|m_1-m_2|}(k\to s)_{ji} \times \tilde{\gamma}_{\mu\nu}(k_i;l_1m_1l_2m_2). \qquad (27)$$

Here the difficulty comes: in the bilayer case we have the Hankel transforms of even and odd orders, and they are all

coupled (see below (30)) and hence must be evaluated on the same grid. However, the conventional algorithm of Lado[6] and Hoffmann[37] for numerical Hankel transforms does not allow to mix the Hankel transforms of different parity on the same grid. We have devised a numerical algorithm to cope with this complication and the reader is referred to Appendix A for details in order not to overburden the presentation. The matrices $B_m(s \to k)$ and $B_m(k \to s)$ for Hankel transform of order m are precomputed and stored before the actual computation starts.

Having expanded the pair functions into the generalized spherical harmonics and applied the Fourier transform operation, the OZ equation (9) gets the form

$$\tilde{\gamma}_{\mu_1\mu_2}(k; l_1m_1l_2m_2) = \rho \sum_{\mu_3, l_3, m_3} (-1)^{m_3} [\tilde{\gamma}_{\mu_1\mu_3}(k; l_1m_1l_3m_3) + \tilde{c}_{\mu_1\mu_3}(k; l_1m_1l_3m_3)] \times \tilde{c}_{\mu_3\mu_2}(k; l_3m_3l_2m_2). \quad (28)$$

Introducing the matrix notation for the expansion coefficients

$$\tilde{\Gamma}(k)_{(\mu_1l_1m_1),(\mu_2l_2m_2)} = \tilde{\gamma}_{\mu_1\mu_2}(k; l_1m_1l_2m_2), \quad (29)$$

we solve (28) for $\tilde{\Gamma}(k)$ as

$$\tilde{\Gamma}(k) = \rho\tilde{C}(k) J \tilde{C}(k) [I - \rho J \tilde{C}(k)]^{-1}, \quad (30)$$

Here I is the unity matrix and

$$J_{(\mu_1l_1m_1),(\mu_2l_2m_2)} = \delta_{\mu_1\mu_2}\delta_{l_1l_2}\delta_{m_1m_2}(-1)^{m_1}. \quad (31)$$

The direct correlation function at large distance s behaves asymptotically as the potential,

$$c_{\mu_1\mu_2}(s; l_1m_1l_2m_2) \sim -\beta u_{\mu_1\mu_2}(s; l_1m_1l_2m_2), \quad (32)$$

and hence it has a long range tail. Since the numerical versions of the Hankel transforms are truncated at a finite range, we are in danger of losing numerical accuracy. In order to overcome this difficulty, we subtract from the coefficients c the function with the same long range behaviour but with an analytically known Hankel transform.[6,37] Namely, from the coefficients that transform with $J_0(ks)$ and $J_2(ks)$ kernels we subtract

$$-\beta u^\star(s; l_1m_1l_2m_2) = \beta\mu^2\Phi(l_1m_1l_2m_2)\frac{\alpha^2}{24}s^2 \times \int_0^1 dx\, x^4 \exp(-\alpha s\, x). \quad (33)$$

From the coefficients that transform with a $J_4(ks)$ kernel we subtract

$$-\beta u^\star(s; l_1m_1l_2m_2) = \beta\mu^2\Phi(l_1m_1l_2m_2)\frac{\alpha^7}{720}s^4 \times \int_0^1 dx\, x^6 \exp(-\alpha s\, x), \quad (34)$$

and from the coefficients that transform with a $J_6(kr)$ kernel we subtract

$$-\beta u^\star(s; l_1m_1l_2m_2) = \beta\mu^2\Phi(l_1m_1l_2m_2)\frac{\alpha^9}{40320}s^6 \times \int_0^1 dx\, x^8 \exp(-\alpha s\, x). \quad (35)$$

Here $\Phi(l_1m_1l_2m_2)$ is a generalized spherical expansion coefficient of $3(\hat{\boldsymbol{\mu}}_i \cdot \hat{\mathbf{s}}_{ij})(\hat{\boldsymbol{\mu}}_j \cdot \hat{\mathbf{s}}_{ij}) - \hat{\boldsymbol{\mu}}_i \cdot \hat{\boldsymbol{\mu}}_j$. The resulting coefficients $c^\star_{\mu_1\mu_2}(s; l_1m_1l_2m_2) = c_{\mu_1\mu_2}(s; l_1m_1l_2m_2) + \beta u^\star(s; l_1m_1l_2m_2)$ are short-ranged. We perform the numerical Hankel transforms of the $c^\star_{\mu_1\mu_2}(s; l_1m_1l_2m_2)$ and add back to them the corresponding analytical transforms of (33)–(35). We will not burden the text with the explicit expressions for $u^\star$ since they can be readily obtained in any symbolic computation suite such as Maple or Mathematica. The numerical parameter α was chosen to be 1.4.

We go back to the KBGY equation (8) and rewrite it in terms of the generalized Legendre functions $\mathcal{P}_{lm}(\cos\theta)$,[6]

$$\frac{d}{dx}\ln[f(x)] = \sum_{l_1,l_2,m} \xi_{l_1,l_2,m}\mathcal{P}_{l_1m}(x)\frac{d\mathcal{P}_{l_2m}(x)}{dx}, \quad (36)$$

$$\xi_{l_1,l_2,m} = -\rho\int d\boldsymbol{s} \sum_{\mu,l_3,m_3} g_{b\mu}(s; l_1ml_3m_3) \times \beta u_{b\mu}(s; l_2ml_3m_3), \quad (37)$$

where $u_{b\mu}(s;\, l_1ml_3m_3)$ are the expansion coefficients of the pair potential $u_{b\mu}(\boldsymbol{s}, \omega, \omega')$. In order to solve (36) with respect to $f(x)$ we expand the $\ln[f(x)]$ as

$$\ln[f(x)] = \sum_{l=1}^{\infty} y_l\mathcal{P}_{l0}(x) + \text{const}, \quad (38)$$

where the constant term is determined from the normalization condition for $f(x)$. We insert (38) into Eq. (36) and after expanding both sides of the equality into generalized Legendre polynomials, we find

$$y_l = \sum_{l_3}[D^{-1}]_{ll_3}\int dx \sum_{l_1,l_2,m} \xi_{l_1,l_2,m}\mathcal{P}_{l_1m}(x) \times \frac{d\mathcal{P}_{l_2m}(x)}{dx}\mathcal{P}_{l_30}(x), \quad (39)$$

where the matrix D is

$$D_{l_1l_2} = \int dx\, \mathcal{P}_{l_10}(x)\frac{d\mathcal{P}_{l_20}(x)}{dx}. \quad (40)$$

The derivatives $\frac{d\mathcal{P}_{lm}(x)}{dx}$ are found from differentiation of the definition of $\mathcal{P}_{lm}$ (18) and of the recursion relation (20).

Now we need to solve Eqs. (10), (30), (38), and (39) for the full system and for the reference system with the closure (12). In the work of Lomba *et al.*,[6] the solution is found by the Picard iterations. In this paper, we use the Newton-GRMES algorithm as implemented in the public-domain Newton iterative solver NITSOL.[26] In order to apply the algorithm we

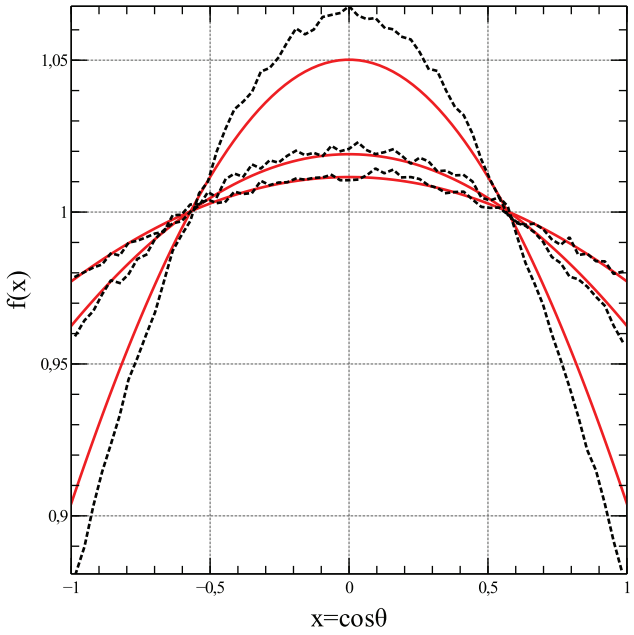

FIG. 1. Orientational distribution functions of dipolar moments in a bilayer of dipolar soft spheres at $T = 1.0$, $\mu = 1.0$, and $h = 1.0$. Red solid lines are RHNC and black dotted lines are MC data. The curves correspond to surface densities $\rho = 0.3$, 0.4, and 0.6 in the order of increasing extremum heights.

need to define the iteration functions and the nonlinear residual functions. We refer the interested reader to Appendix B for the details.

III. MONTE CARLO SIMULATION

The MC simulations were carried out in the canonical (NVT) ensemble with $N = 288$ particles equally distributed among two square layers with sides L. The layers are separated by the distance h. The simulation box formed by these layers has periodic boundary conditions (PBCs) along x and y directions and no PBCs are taken along z direction. The total number of steps was about 10^6, each step consisting of sequential displacement, rotation and inversion of all the particles. The amplitude of the trial moves was chosen to maintain the acceptance ratio between 25% and 75%. The dipolar part of the potential energy was computed by the 2D Ewald summation method EW2D + h.[38] Note that there is a typo in Ref. 38 in the formulas and we refer the reader to the work[19] for explicit expressions. All the Ewald method parameters were setup according to Ref. 19.

IV. RESULTS AND CONCLUSION

In order to test the theory developed here, the RHNC equations where solved for the bilayer system consisting of particles with dipole moment $\mu = 1.0$ on monolayers separated by distance $h = 1.0$ at inverse temperature $\beta = 1.0$. We considered the cases for surface densities $\rho = 0.3$, 0.4, and 0.6. The one-particle angular distribution functions are presented in Fig. 1. It is seen that up to $\rho = 0.4$ they agree well with Monte Carlo results. It is known that when the dipolar interaction becomes stronger, the dipoles are predominantly oriented in plane[19] and the distribution functions have distinct peak around $\cos\theta = 0$. However in the case of $\mu = 1.0$ treated here the interaction is not so strong, and the distribution functions on Fig. 1 are almost flat, i.e., the dipoles orient almost freely in space.

Structural properties of the bilayer are characterized by the angle-averaged center-to-center intra- and interlayer pair distribution functions,

$$g_{\mu\nu}^{000}(s) = \langle g_{\mu\nu}(\boldsymbol{s}, \omega_1, \omega_2)\rangle_{\omega_1\omega_2} = g_{\mu\nu}(s; 0000), \tag{41}$$

which are presented in Fig. 2 for intralayer case and in Fig. 3 for interlayer case. It is seen that in the intralayer case the distribution functions agree with Monte Carlo almost quantitatively up to $\rho = 0.4$. However in the interlayer case small discrepancies are seen. To interpret the results in Figs. 2 and 3, we note that if $h = 0$, then $g_{bb}^{000}(s) = g_{bt}^{000}(s)$, and they both would be equal to the distribution function of monolayer at the density 2ρ. If we start to increase h from zero, this can be thought of as if the half of the particles in the monolayer, the t species, would become penetrable and smeared out with respect to another half, the b-species. That is why $g_{bt}^{000}(s)$ is not zero and increasing in the neighborhood of $s = 0$, and has the smaller peak heights, in contrast to $g_{bb}^{000}(s)$. The peaks in $g_{bt}^{000}(s)$ are also shifted to smaller s with respect to $g_{bb}^{000}(s)$ since t-species can come closer to b-species than b-species to b-species.

The orientational properties are characterized by the projections of distribution function onto standard rotational invariants.[6,19] We compute the two most important projections, $h_{\mu\nu}^{110}(s)$ and $h_{\mu\nu}^{112}(s)$.[6] They are defined as

$$\begin{aligned} h_{bb}^{110}(s) &= 3\langle g_{bb}(\boldsymbol{s}, \omega_1, \omega_2)(\hat{\boldsymbol{\mu}}_1 \cdot \hat{\boldsymbol{\mu}}_2)\rangle_{\omega_1\omega_2} \\ &= 3[\langle x\rangle^2 g_{bb}(s; 0000) + \sigma\langle x\rangle\{g_{bb}(s; 1000) + g_{bb}(s; 0010)\} + \sigma^2 g_{bb}(s; 1010) \\ &\quad + \{\langle x^2\rangle - 1\} g_{bb}(s; 1111)], \end{aligned} \tag{42}$$

$$\begin{aligned} h_{bb}^{112}(s) &= \frac{3}{2}\langle g_{bb}(\boldsymbol{s}, \omega_1, \omega_2)[3(\hat{\boldsymbol{\mu}}_1 \cdot \hat{\mathbf{s}})(\hat{\boldsymbol{\mu}}_2 \cdot \hat{\mathbf{s}}) - (\hat{\boldsymbol{\mu}}_1 \cdot \hat{\boldsymbol{\mu}}_2)]\rangle_{\omega_1\omega_2} \\ &= -\frac{3}{2}\Bigg[\langle x\rangle^2 g_{bb}(s; 0000) + \sigma\langle x\rangle\{g_{bb}(s; 1000) + g_{\mu\nu}(s; 0010)\} + \sigma^2 g_{bb}(s; 1010) \\ &\quad + \{1 - \langle x^2\rangle\}\left\{\frac{1}{2} g_{bb}(s; 1111) - \frac{3}{4}(g_{bb}(s; 1\bar{1}11) + g_{bb}(s; 111\bar{1})\right\}\Bigg], \end{aligned} \tag{43}$$

for the intralayer case, and

$$h_{bt}^{110}(s) = 3\langle g_{bt}(\boldsymbol{s},\omega_1,\omega_2)(\hat{\boldsymbol{\mu}}_1\cdot S\hat{\boldsymbol{\mu}}_2)\rangle_{\omega_1\omega_2}$$
$$= 3[-\langle x\rangle^2 g_{bt}(s;0000) - \sigma\langle x\rangle\{g_{bt}(s;1000)+g_{bt}(s;0010)\} - \sigma^2 g_{bt}(s;1010)$$
$$+\{\langle x^2\rangle - 1\}g_{bt}(s;1111)], \tag{44}$$

$$h_{bt}^{112}(s) = \frac{3}{2}\langle g_{bt}(\boldsymbol{s},\omega_1,\omega_2)[3(\hat{\boldsymbol{\mu}}_1\cdot\hat{\boldsymbol{r}})(S\hat{\boldsymbol{\mu}}_2\cdot\hat{\boldsymbol{r}}) - (\hat{\boldsymbol{\mu}}_1\cdot S\hat{\boldsymbol{\mu}}_2)]\rangle_{\omega_1\omega_2}$$
$$= -\frac{3}{2}\left[\left(3\frac{h^2}{s^2+h^2}-1\right)\right.$$
$$\times\{\langle x\rangle^2 g_{bt}(s;0000)+\sigma\langle x\rangle(g_{bt}(s;1000)+g_{bt}(s;0010))+\sigma^2 g_{bt}(s;1010)\}$$
$$+(1-\langle x^2\rangle)\left\{\left(\frac{3}{2}\frac{s^2}{s^2+h^2}-1\right)g_{bt}(s;1111) - \frac{3}{2}\frac{s^2}{s^2+h^2}g_{bt}(s;1\bar{1}11)\right\}$$
$$+3\frac{sh}{s^2+h^2}\sqrt{1-\langle x^2\rangle}$$
$$\left.\times\ \{\sigma(g_{bt}(s;1110)+g_{bt}(s;1011))+\langle x\rangle(g_{bt}(s;1100)+g_{bt}(s;0011))\}\right], \tag{45}$$

for the interlayer case. Note that in the definitions of $h_{bt}^{110}(s)$ (44) and h_{bt}^{112} (45), we reflect the dipole moment $\hat{\boldsymbol{\mu}}_2$ so that we calculate the rotational invariant of the original bilayer system, rather than the mapped monolayer one. The projections h_{bb}^{110} and h_{bt}^{110} characterize the degree of correlation in orientations of the dipole pair at a distance s. Here $\langle x\rangle = \frac{1}{2}\int f(x)xdx$, $\langle x^2\rangle = \frac{1}{2}\int f(x)x^2dx$, and $\sigma^2 = \langle x^2\rangle - \langle x\rangle^2$. The results for the intralayer case are presented in Fig. 4, and for the interlayer case in Fig. 5.

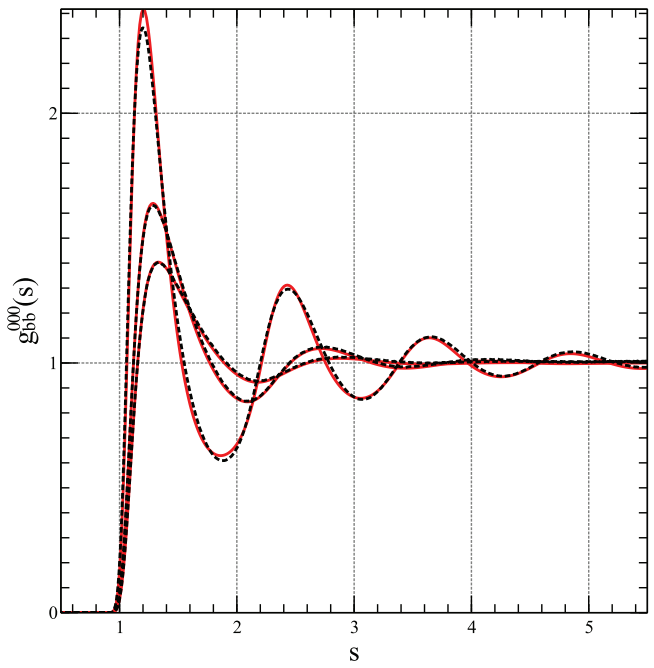

FIG. 2. Intralayer angle-averaged pair distribution function for the same system as in Fig. 1. The curves correspond to surface densities $\rho = 0.3$, 0.4, and 0.6 in the order of increasing first peak heights.

The projections h_{bb}^{112} and h_{bt}^{112} carry information on thermodynamical properties of the system. The results for the intralayer case are presented in Fig. 6 and for the interlayer case in Fig. 7. The results in Figs. 6 and 7 can be interpreted using the same picture as we have used above for distribution functions. The first peak in the orientation pair functions indicates that the neighboring particles (in the same or in different layers) tend to orient in the same direction.

It would be interesting to see how the theory compares to Monte Carlo simulations at higher dipolar moments μ when the dipoles are predominantly oriented in the plane. In case

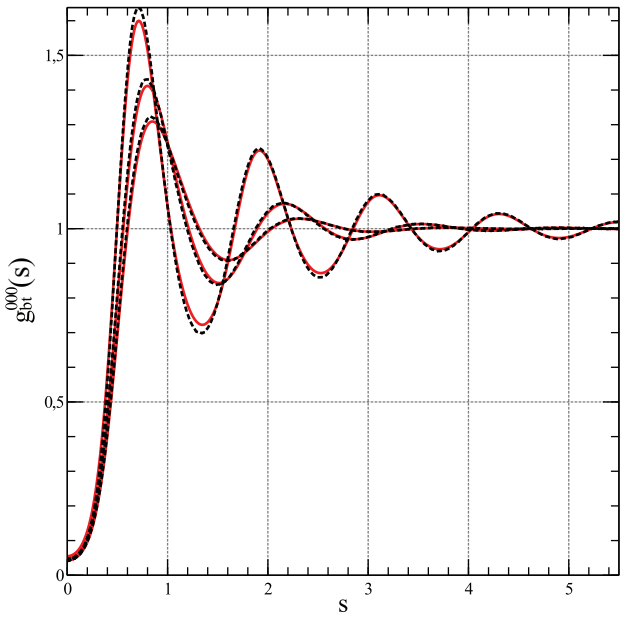

FIG. 3. Interlayer angle-averaged pair distribution function for the same system and parameters as in Fig. 2.

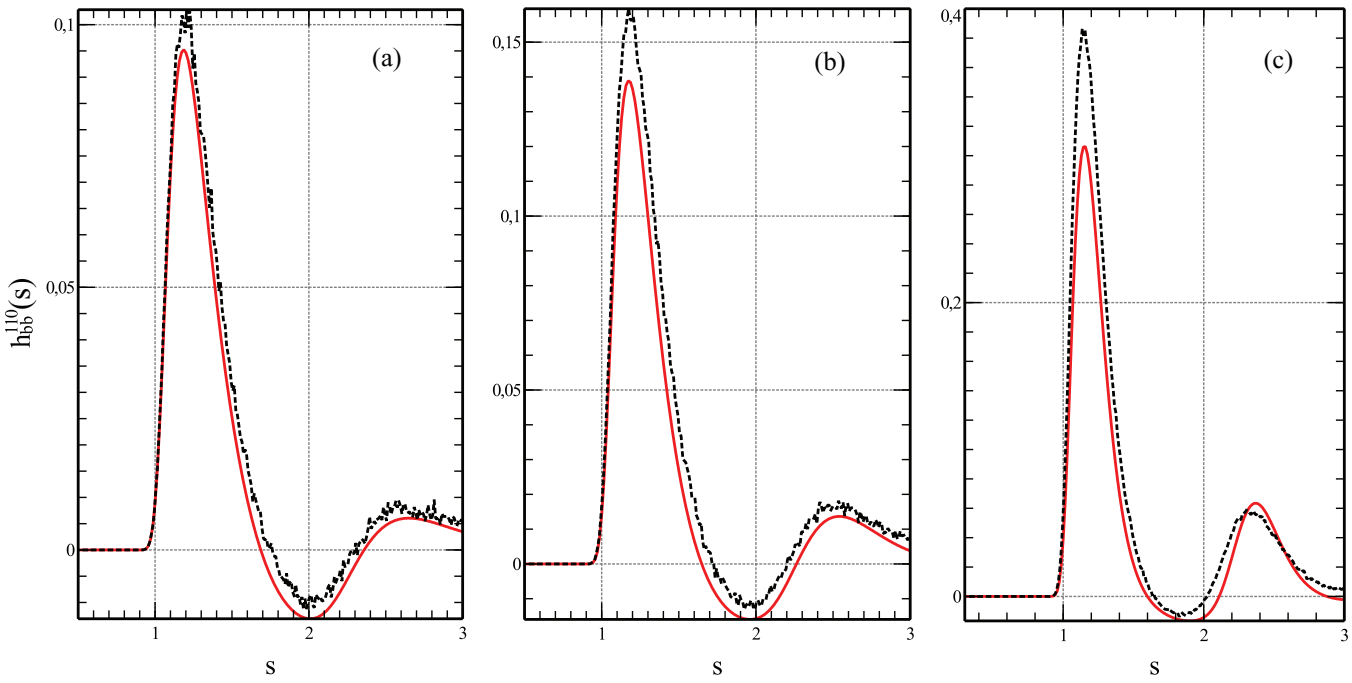

FIG. 4. Projection of intralayer pair distribution function $h_{bb}^{110}(s)$ for the same system as in Fig. 1; (a) at surface density $\rho = 0.3$; (b) at surface density $\rho = 0.4$; (c) at surface density $\rho = 0.6$.

of density values $\rho = 0.3$, 0.4, and 0.6, we have achieved the convergence of RHNC equations up to $\mu \approx 1.9$ by gradually increasing μ starting from the value of 1.0. Above the value $\mu \approx 1.9$, the convergence becomes extremely slow, and we did not wait for the results. Whereas the value of $\mu = 1.9$ is not high enough to reach the mode of inplane dipole orientation, we encounter problems also with Monte Carlo: starting from $\mu \approx 1.9$ strong dependence on sample size is observed. We have tried the particle numbers $N = 288$, 576, 1152, and each time the shape of the pair functions changes considerably. More over, h_{bb}^{110} has a slowly decaying tail which oscillates as the sample size is changed. So the quantitative comparison to RHNC is not possible. To clarify what is happening, e.g., a phase transition, some structural reorganization, inefficient Monte Carlo sampling, or a need to take much bigger simulation sample, an additional research is required.

In conclusion, the RHNC theory was extended to the case of the bilayer of dipolar particles. The procedure of numerical

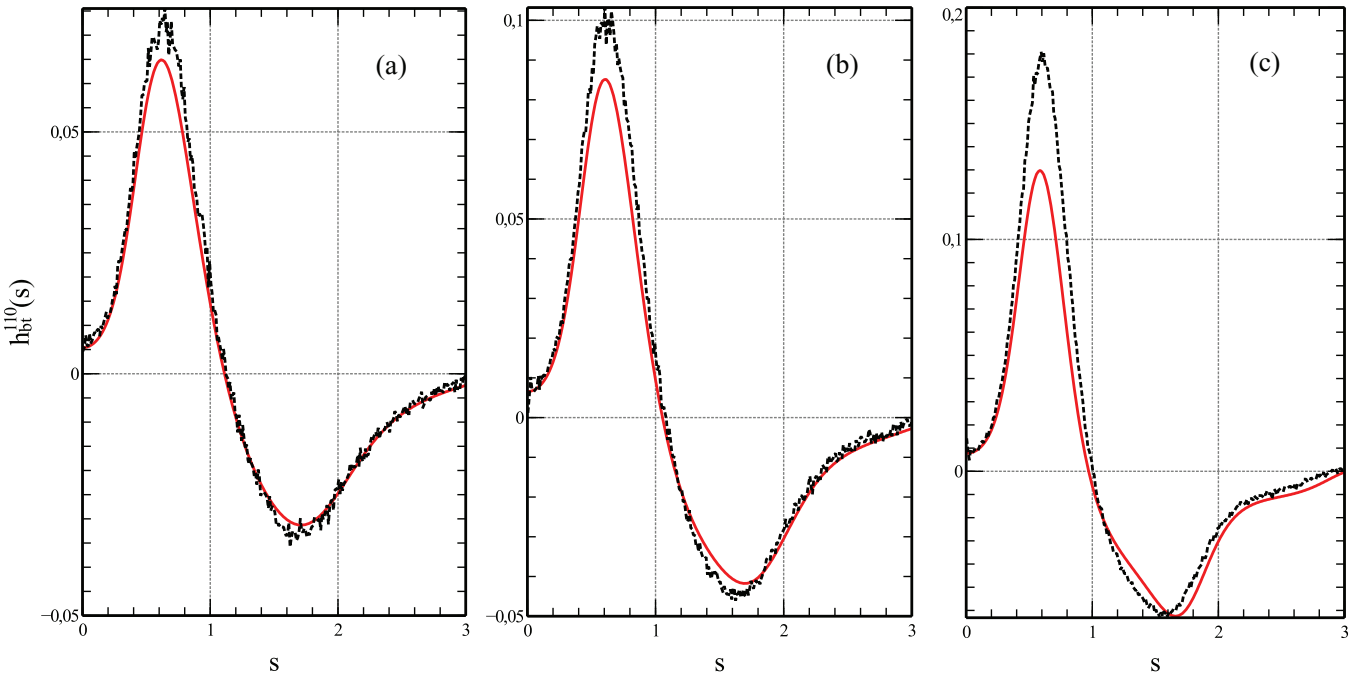

FIG. 5. Projection of intralayer pair distribution function $h_{bt}^{110}(s)$ for the same system as in Fig. 1; (a) at surface density $\rho = 0.3$; (b) at surface density $\rho = 0.4$; (c) at surface density $\rho = 0.6$.

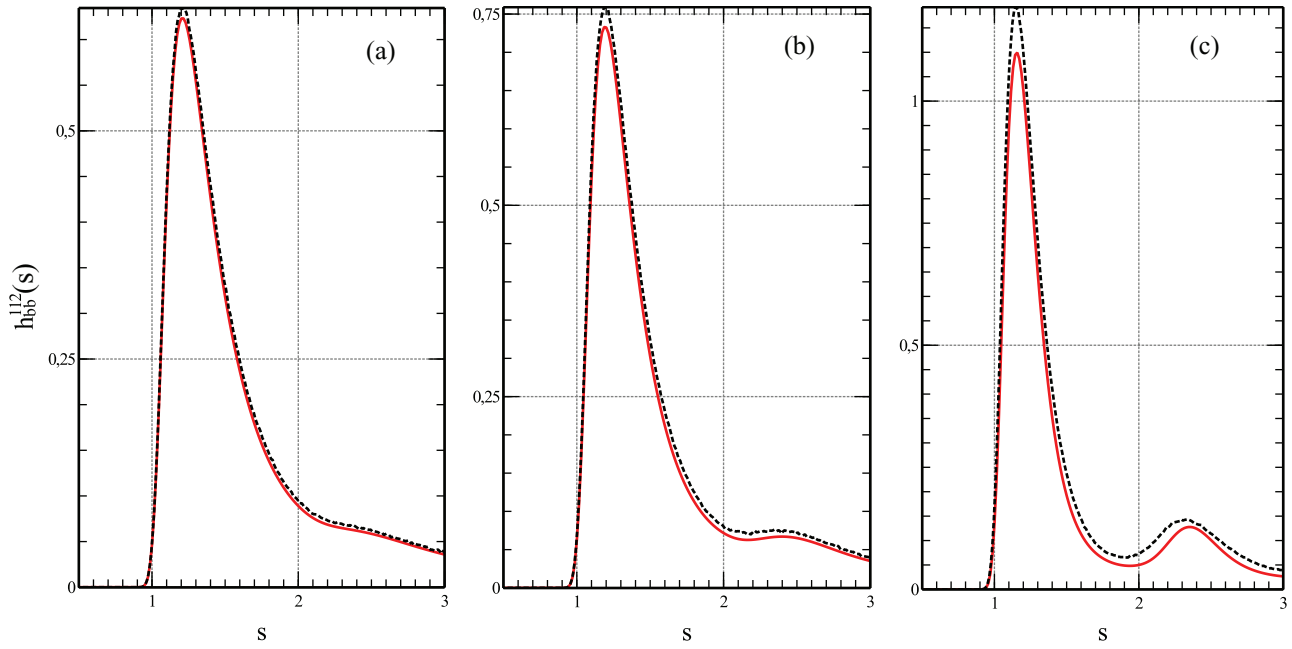

FIG. 6. Projection of intralayer pair distribution function $h_{bb}^{112}(s)$ for the same system as in Fig. 1; (a) at surface density $\rho = 0.3$; (b) at surface density $\rho = 0.4$; (c) at surface density $\rho = 0.6$.

solution using the Newton-GRMES method is presented and validated on several test calculations. The isotropic center-to-center distribution for intralayer case is in good agreement with Monte Carlo up to $\rho = 0.4$ but for interlayer case we clearly see the discrepancies. The projections onto rotational invariants h^{112} are reproduced much better than h^{110} in intralayer case, and again the interlayer projections are worse than intralayer ones. It looks like in the hard-spheres monolayer case the RHNC gives slightly better orientational pair functions[6] at the intermediate densities $\rho \approx 0.4$. We believe that this can be explained by the influence of two factors. First, at the same surface density the soft sphere monolayer system is effectively denser than the hard sphere one treated in Ref. 6. This can be seen from the center-to-center distribution function which is more structured for the soft sphere system. Then, in the bilayer case the repulsion from the second monolayer also makes the system effectively denser. The other factor is that in the bilayer case the pressure-consistent closure (the reference system calculation) works slightly worse for interlayer distribution functions. Perhaps the reason is that in the monolayer case we have only the lateral pressure, and the PC closure achieves consistency in it. However in the bilayer

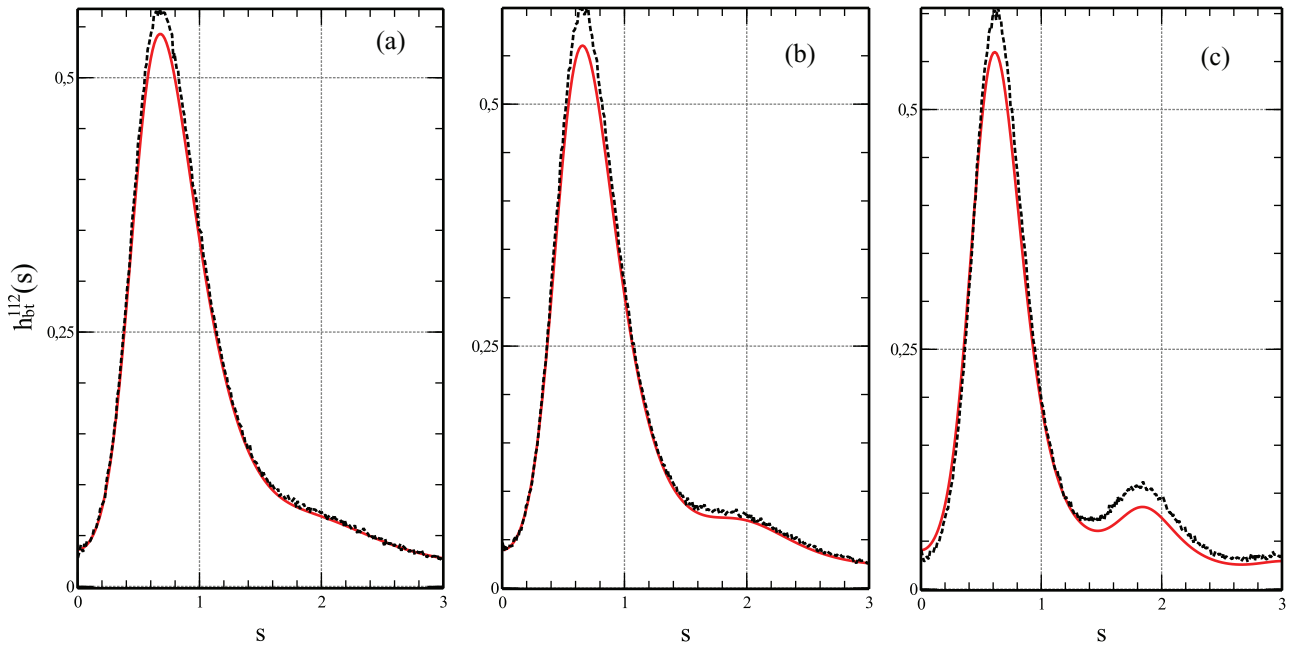

FIG. 7. Projection of intralayer pair distribution function $h_{bb}^{112}(s)$ for the same system as in Fig. 1; (a) at surface density $\rho = 0.3$; (b) at surface density $\rho = 0.4$; (c) at surface density $\rho = 0.6$.

case we have also the normal pressure which reflects interaction between the monolayers. So one possible direction of research is to extend the notion of thermodynamic consistency on the normal pressure, and to generalize the PC closure appropriately, in the hope that this will improve the interlayer reference distribution functions and hence the bridge functions. Besides that, in this paper we compute only the distribution functions for the bilayer since here we are focusing our efforts to extend the formalism onto bilayer case. However, there are a lot more thermodynamic properties that should be investigated: the internal energy; the normal and the lateral pressure; the dependence of the interaction between the monolayers upon the external or pair potentials acting upon the soft spheres. More over, work currently is underway to include the point charges between the monolayers into the RHNC framework, to model theoretically the interaction between the (spatial charge) double layer and the dipolar structure of the interface surfaces.

ACKNOWLEDGMENTS

This work is supported by the program of grants for postdocs of St. Petersburg State University (Grant No. 11.50.1573.2013) and by the Russian Foundation for Basic Research (Grant No. 14-02-31109).

APPENDIX A: NUMERICAL HANKEL TRANSFORMS

To the authors' knowledge, in the liquid structure calculations in planar setup there occur the Hankel transforms of even order only. And the most robust algorithm is for $J_0(ks)$-transform which has been devised by Lado,[39] and more than two decades later was rediscovered by Yu *et al.*[40] The transforms of higher (even) order are reduced to zero order transform by special "raising" and "lowering" operations.[6,37]

According to Lado's recipe,[39] we assume that the function $f(s)$ is defined for $s \geq 0$, that $f(s)$ vanishes for $s \geq S$, and that its Fourier (Hankel) transform $\tilde{f}(k)$ vanishes for $k \geq K$, i.e., the function is band-limited both in space and in frequency. Then the discrete version of the zero-order Hankel transforms (24), (25) is

$$\tilde{f}\left(k_p^{(0)}\right) = \frac{4\pi}{K^2} \sum_{q=1}^{N-1} f\left(s_q^{(0)}\right) \frac{J_0\left(k_p^{(0)} s_q^{(0)}\right)}{\left[J_1\left(K s_q^{(0)}\right)\right]^2}, \tag{A1}$$

$$f\left(s_p^{(0)}\right) = \frac{1}{\pi S^2} \sum_{q=1}^{N-1} \tilde{f}\left(k_q^{(0)}\right) \frac{J_0\left(k_q^{(0)} s_p^{(0)}\right)}{\left[J_1\left(k_q^{(0)} S\right)\right]^2}. \tag{A2}$$

Here

$$s_p^{(0)} = \frac{\eta_p^{(0)}}{\eta_N^{(0)}} S, \quad k_p^{(0)} = \frac{\eta_p^{(0)}}{S} \tag{A3}$$

are the zero-order Bessel grid points in space and in frequency domain correspondingly; $\eta_p^{(0)}$ is the p-th positive root of $J_0(s)$; the spectral cut-off $K = k_N$. This algorithm is very accurate and now has become a standard in the field of planar liquid structure calculations.

After a while in the field of optics, a generalization of the Lado's recipe was done for arbitrary integer order Hankel transform.[41] Under the same assumptions about the function $f(s)$, the discrete m-order transform is

$$\tilde{f}\left(k_p^{(m)}\right) = i^m \frac{4\pi}{K^2} \sum_{q=1}^{N-1} f\left(s_q^{(m)}\right) \frac{J_m\left(k_p^{(m)} s_q^{(m)}\right)}{\left[J_{m+1}\left(K s_q^{(m)}\right)\right]^2}, \tag{A4}$$

$$f\left(s_p^{(m)}\right) = i^{-m} \frac{1}{\pi S^2} \sum_{q=1}^{N-1} \tilde{f}\left(k_q^{(m)}\right) \frac{J_m\left(k_q^{(m)} s_p^{(m)}\right)}{\left[J_{m+1}\left(k_q^{(m)} S\right)\right]^2}. \tag{A5}$$

Here

$$s_p^{(m)} = \frac{\eta_p^{(m)}}{\eta_N^{(m)}} S, \quad k_p^{(m)} = \frac{\eta_p^{(m)}}{S} \tag{A6}$$

are the m-order Bessel grid points in space and in frequency domain correspondingly; $\eta_p^{(m)}$ is the pth positive root of $J_m(s)$; the spectral cut-off $K = k_N$; i is imaginary unit. The accuracy of the algorithm is the same[41] as that of the original Lado's recipe.

The algorithm of Lado is quite popular in liquid structure calculation because it would be exact for the functions which are band-limited both in space and in frequency (if such functions existed), and in physics we usually have functions $f(s)$ which are extremely close to this class (after having subtracted analytically the cusps, discontinuities, and tails if necessary). We would like to devise an algorithm for integer order Hankel transforms on a common grid with the same accuracy characteristics as in the original Lado approach.

The discrete transforms (A1)–(A5) are defined on the Bessel grid, and it is known that the band-limited functions (in Hankel transform sense) can be discretized on Bessel grids without the loss of information.[42,43] More precisely, there is a theorem: if function $f(s)$ is band-limited to $[0, K]$ in frequency then it has the following sampling expansion:[42]

$$f(s) = \sum_{p=1}^{\infty} \frac{2\eta_p^{(m)} J_m(Ks)}{J_{m+1}\left(\eta_p^{(m)}\right)\left(\eta_p^{(m)2} - K^2 s^2\right)} f\left(s_p^{(m)}\right). \tag{A7}$$

Similarly in frequency domain we have

$$f(k) = \sum_{p=1}^{\infty} \frac{2\eta_p^{(m)} J_m(Sk)}{J_{m+1}\left(\eta_p^{(m)}\right)\left(\eta_p^{(m)2} - S^2 k^2\right)} f\left(k_p^{(m)}\right). \tag{A8}$$

So if we define such a function on the Bessel grid, we can freely interpolate between the grid points.

Now since we have the discrete transforms (A4)–(A5), each defined on its own grid, we could choose one common grid, e.g., zero-order Bessel grid, and discretize the s-dependence of all the pair functions on it. Then when calculating m-order Hankel transform, we could first interpolate from the zero-order Bessel grid to m-order grid using (A7) or (A8), then perform the transform using (A4) or (A5), and interpolate back to the zero-order grid. However having carried out a number of numerical experiments we are led to the conclusion that this procedure is not robust. Here are our empirical findings:

(1) Interpolation from the even order Bessel grid is robust if $f(s)$ is even with high accuracy. Practically this means that the leading terms in the Taylor expansion around zero should be even powers of s.

(2) Interpolation from the odd order Bessel grid is robust if $f(s)$ is odd with high accuracy. Practically this means that the leading terms in the Taylor expansion around zero should be odd powers of s.
(3) Interpolation from the m-order Bessel grid is robust if $f(s)$ behaves as $O(s^m)$ at $s = 0$.

The same considerations apply to the accuracy of discrete transforms (A4), (A5). In fact, all these observations can be understood if we look at (A7) and take into account that $J_m(Ks) \sim (Ks/2)^m/\Gamma(m+1)$ at $s = 0$, and its Taylor expansion is only in even or only in odd powers, in accordance with the parity of m.

At first glance, based on the facts (1)–(3), one can conclude that the discrete transforms (A4)–(A5) are useless for $m > 0$. However, the situation is not as hopeless. The key point here is that for any given pair function h we perform the Hankel transform of order m only on the generalized spherical expansion coefficient $h(s; l_1 m_1 l_2 m_2)$ with $m_1 - m_2 = m$. So if the $\boldsymbol{s}$-vector dependence of h can be expanded into Taylor series around $\boldsymbol{s} = 0$, then we have

$$\begin{aligned} h(\boldsymbol{s};\cdots) &= \sum_{mn} \frac{h^{(m,n)}(\cdots)}{m!n!} s_x^m s_y^n \\ &= \sum_{mn} \frac{h^{(m,n)}(\cdots)}{m!n!} s^{m+n} \\ &\quad \times \cos^m \phi_s \sin^n \phi_s . \end{aligned} \tag{A9}$$

This means that if $h(s)$ is smooth enough, then

$$h(s; l_1 m_1 l_2 m_2) \sim s^{|m_1 - m_2|} \tag{A10}$$

at $s = 0$, and the criteria (1)–(3) above are satisfied. The discrete transforms (A4)–(A5) of order m are thus robust for the corresponding generalized spherical expansion coefficient. The only remaining task is to devise a common grid, from which we can reliably interpolate irrespectively of the asymoptic behaviour at $s = 0$. We have chosen the uniform grid

$$s_i = \frac{i-1}{N-1} S, \quad k_i = \frac{i-1}{N-1} \frac{\pi}{S}, \quad K = k_N, \quad i = 1 \ldots N \tag{A11}$$

as a common grid, and according to the Whittaker–Shannon interpolation formula

$$\begin{aligned} f(s) = \sum_{i=1}^{N} f(s_i) \Bigg\{ & \frac{\sin\left[\frac{\pi}{\Delta s}(s - s_i)\right]}{\frac{\pi}{\Delta s}(s - s_i)} \\ & \pm \frac{\sin\left[\frac{\pi}{\Delta s}(s + s_i)\right]}{\frac{\pi}{\Delta s}(s + s_i)} \Bigg\} \end{aligned} \tag{A12}$$

and

$$\begin{aligned} f(k) = \sum_{i=1}^{N} f(k_i) \Bigg\{ & \frac{\sin\left[\frac{\pi}{\Delta k}(k - k_i)\right]}{\frac{\pi}{\Delta k}(k - k_i)} \\ & \pm \frac{\sin\left[\frac{\pi}{\Delta k}(k + k_i)\right]}{\frac{\pi}{\Delta k}(k + k_i)} \Bigg\}, \end{aligned} \tag{A13}$$

which are exact for band-limited functions (in the Fourier transform sense). Here the plus signs are taken for even f, hence even m, and the minus signs are taken for odd f, hence odd m. Note that all the transform and interpolation relations (A4)–(A13) can be represented as matrix multiplications. Then we have for the discrete transform matrices $B_m(s \to k)$ and $B_m(s \to k)$,

$$B_m(s \to k) = B_k(m)\, H(m; s \to k)\, U_s(m), \tag{A14}$$

$$B_m(k \to s) = B_s(m)\, H(m; k \to s)\, U_k(m), \tag{A15}$$

where $U_s(m)$ and $U_k(m)$ are the matrices corresponding to interpolation from uniform to m-order Bessel grid in space (subscript s) and frequency (subscript k) domain; $B_k(m)$ and $B_s(m)$ correspond to interpolation from m-order Bessel to uniform grid in space (subscript s) and frequency (subscript k) domain; $H(m; s \to k)$ and $H(m; k \to s)$ are the matrices of the discrete transforms (A4) and (A5) of order m. Note that the transforms (A14) and (A15) yield the same accuracy as the original Lado approach (A1)–(A2) provided that the asymptotics (A10) holds.

APPENDIX B: SUMMARY OF NUMERICAL PROCEDURE

The solution of RHNC equations involves two stages. First, we solve the pressure-consistent integral equation for the reference system. We do it in terms of the variables $P_{\mu\nu}$, $H_{\mu\nu}$, $C_{\mu\nu}$ which are multicomponent generalization of P, H, C of the Lado's work.[31] The Newton solver's iteration function is chosen to be $H_{\mu\nu}(s) = g^{\mathrm{ref}}_{\mu\nu}(s)\, e^{\beta u^{\mathrm{ref}}_{\mu\nu}(s)} - 1$ and the corresponding nonlinear residual $\delta H_{\mu\nu}(s)$ is calculated through the following steps:

$$P_{\mu\nu}(s) = H_{\mu\nu}(s) - \ln[1 + H_{\mu\nu}(s)], \tag{B1}$$

$$C_{\mu\nu}(s) = [1 + H_{\mu\nu}(s)]\left(e^{-\beta u^{\mathrm{ref}}_{\mu\nu}(s)} - 1\right) + \xi P_{\mu\nu}(s), \tag{B2}$$

$$\tilde{P}_{\mu\nu}(k_j) = \sum_i B_0(s \to k)_{ji}\, P_{\mu\nu}(s_i), \tag{B3}$$

$$\tilde{C}_{\mu\nu}(k_j) = \sum_i B_0(s \to k)_{ji}\, C_{\mu\nu}(s_i), \tag{B4}$$

$$\tilde{H}(k) = \xi \tilde{P}(k) + \rho \tilde{C}(k)\, \tilde{C}(k)\, [1 - \rho \tilde{C}(k)]^{-1}, \tag{B5}$$

where $\tilde{H}(k)$, $\tilde{C}(k)$, and $\tilde{P}(k)$ are matrices with the elements $\tilde{H}_{\mu\nu}(k)$, $\tilde{C}_{\mu\nu}(k)$, and $\tilde{P}_{\mu\nu}(k)$ correspondingly,

$$H_{\mu\nu(\mathrm{next})}(s_j) = \sum_i B_0(k \to s)_{ji}\, \tilde{H}_{\mu\nu}(k_i), \tag{B6}$$

$$\delta H_{\mu\nu}(s) = H_{\mu\nu(\mathrm{next})}(s) - H_{\mu\nu}(s). \tag{B7}$$

After the solution is converged, the bridge functions are calculated as

$$b_{\mu\nu}(s) = (\xi - 1)\, P_{\mu\nu}(s). \tag{B8}$$

Next the RHNC system is solved. We choose the iteration functions to be $y_1(x) = \ln[f(x)]$, $\gamma_{bb}(s, x_1, x_2, \phi_1, \phi_2)$, $\gamma_{bt}(s, x_1, x_2, \phi_1, \phi_2)$, and $\eta = \ln\{2/\int dx \exp[y_1(x)]\}$. Here the function $y_1(x)$ is defined on the reference grid and the x-dependence of the other functions is defined on the adaptive grid. The function η is used to ensure that the converged $f(x)$ will have proper normalization. Given a set of estimates for iteration functions, the nonlinear residuals δy_1, $\delta\gamma_{bb}$, $\delta\gamma_{bt}$, η for our system of integral equations are calculated by the following steps:

(1) Orientational distribution function $f(x)$ is calculated from $y_1(x)$ on the reference grid,

$$f(x) = \exp[\eta + y_1(x)], \tag{B9}$$

where

$$\eta = \ln\left\{2 \Big/ \int dx \, \exp[y_1(x)]\right\} \tag{B10}$$

is one of the residual outputs (the value of η on input is ignored).

(2) A set of generalized spherical harmonics $\mathcal{Y}_{lm}(\omega)$ and the corresponding adaptive quadrature weights ω_i and grid points x_i are calculated for the current $f(x)$. All the other input iteration functions are regarded as defined on this adaptive grid.

(3) Updated estimates of indirect correlation functions $\gamma_{bb(\text{next})}$, $\gamma_{bt(\text{next})}$ are calculated,

$$g_{\mu\nu}(s, x_1, x_2, \phi_1, \phi_2) = \exp[-\beta u_{\mu\nu}(s, x_1, x_2, \phi_1, \phi_2) + \gamma_{\mu\nu}(s, x_1, x_2, \phi_1, \phi_2) + b_{\mu\nu}(s)], \tag{B11}$$

$$c_{\mu\nu}(s, x_1, x_2, \phi_1, \phi_2) = g_{\mu\nu}(s, x_1, x_2, \phi_1, \phi_2) - \gamma_{\mu\nu}(s, x_1, x_2, \phi_1, \phi_2) - 1, \tag{B12}$$

$$\begin{aligned} c_{\mu\nu}(s; l_1 m_1 l_2 m_2) = {} & \frac{1}{16}\frac{1}{(l_{max}+1)^2}(\operatorname{sgn} m_1)^{m_1}(\operatorname{sgn} \bar{m}_2)^{m_2}\frac{1}{\mathcal{N}_{l_1 m_1}\mathcal{N}_{l_2 m_2}}\sum_{i,j}\omega_i\omega_j \\ & \times \left(1 - x_i^2\right)^{|m_1|/2}\mathcal{Q}^{|m_1|}_{l_1-|m_1|}(x_i)\left(1 - x_j^2\right)^{|m_2|/2}\mathcal{Q}^{|m_2|}_{l_2-|m_2|}(x_j) \\ & \times \sum_{pq}\cos(m_1\phi_p - m_2\phi_q)c_{\mu\nu}(s, x_i, x_j, \phi_p, \phi_q), \end{aligned} \tag{B13}$$

$$\tilde{c}_{\mu\nu}(k_j; l_1 m_1 l_2 m_2) = \sum_i B_{|m_1-m_2|}(s \to k)_{ji} c_{\mu\nu}(s_i; l_1 m_1 l_2 m_2), \tag{B14}$$

$$\tilde{\Gamma}_{(\text{next})}(k) = \rho\tilde{C}(k)J\tilde{C}(k)[I - \rho J\tilde{C}(k)]^{-1}, \tag{B15}$$

$$\gamma_{\mu\nu(\text{next})}(s_j; l_1 m_1 l_2 m_2) = \sum_i B_{|m_1-m_2|}(k \to s)_{ji}\tilde{\gamma}_{\mu\nu(\text{next})}(k_i; l_1 m_1 l_2 m_2), \tag{B16}$$

$$\begin{aligned} \gamma_{\mu\nu(\text{next})}(s, x_1, x_2, \phi_1, \phi_2) = {} & \sum_{l_1 m_1}\sum_{l_2 m_2}(\operatorname{sgn} m_1)^{m_1}(\operatorname{sgn} \bar{m}_2)^{m_2}\frac{1}{\mathcal{N}_{l_1 m_1}\mathcal{N}_{l_2 m_2}} \\ & \times \left(1 - x_1^2\right)^{|m_1|/2}\mathcal{Q}^{|m_1|}_{l_1-|m_1|}(x_1)\left(1 - x_2^2\right)^{|m_2|/2}\mathcal{Q}^{|m_2|}_{l_2-|m_2|}(x_2) \\ & \times \cos(m_1\phi_1 - m_2\phi_2)\gamma_{\mu\nu(\text{next})}(s; l_1 m_1 l_2 m_2), \end{aligned} \tag{B17}$$

and

$$\delta\gamma_{\mu\nu}(s, x_1, x_2, \phi_1, \phi_2) = \gamma_{\mu\nu(\text{next})}(s, x_1, x_2, \phi_1, \phi_2) - \gamma_{\mu\nu}(s, x_1, x_2, \phi_1, \phi_2) \tag{B18}$$

are parts of the residual outputs.

(4) Updated estimate of orientational distribution function $f(x)$ is calculated,

$$\begin{aligned} \xi_{l_1, l_2, m} = {} & -\rho\int d\boldsymbol{s}\sum_{\mu, l_3, m_3} g_{b\mu}(s; l_1 m l_3 m_3) \\ & \times \beta u_{b\mu}(s; l_2 m l_3 m_3), \end{aligned} \tag{B19}$$

$$\begin{aligned} y_l = {} & \sum_{l_3}[D^{-1}]_{l l_3}\int dx \sum_{l_1, l_2, m}\xi_{l_1, l_2, m}\mathcal{P}_{l_1 m}(x) \\ & \times \frac{d\mathcal{P}_{l_2 m}(x)}{dx}\mathcal{P}_{l_3 0}(x), \end{aligned} \tag{B20}$$

$$y_{1(\text{next})}(x) = \sum_{l=1}^{\infty} y_l \mathcal{P}_{l0}(x) + \text{const}, \tag{B21}$$

and

$$\delta y_1(x) = y_{1(\text{next})}(x) - y_1(x) \tag{B22}$$

is the last part of the residual outputs. The NITSOL solver has a few more important parameters which we specify. The maximum size of the Krylov subspace is set to 30. Maximum allowable number of backtracks is set to 1000. We use the default values for all the other parameters.

[1]R. Kjellander and S. Sarman, Mol. Phys. **70**, 215 (1990).
[2]H. Greberg and R. Kjellander, Mol. Phys. **83**, 789 (1994).
[3]H. Greberg, R. Kjellander, and T. Åkesson, Mol. Phys. **87**, 407 (1996).
[4]H. Greberg, R. Kjellander, and T. Åkesson, Mol. Phys. **92**, 35 (1997).
[5]R. Kjellander and H. Greberg, J. Electroanal. Chem. **450**, 233 (1998).
[6]E. Lomba, F. Lado, and J. J. Weis, Phys. Rev. E **61**, 3838 (2000).
[7]J. Mingins, D. Stigter, and K. A. Dill, Biophys. J. **61**, 1603 (1992).
[8]D. Stigter, J. Mingins, and K. A. Dill, Biophys. J. **61**, 1616 (1992).
[9]G. J. Zarragoicoechea, Mol. Phys. **96**, 1109 (1999).
[10]E. C. Mbamala, A. Fahr, and S. May, Langmuir **22**, 5129 (2006).
[11]A. Haugen and S. May, J. Chem. Phys. **127**, 215104 (2007).
[12]D. H. Mengistu and S. May, J. Chem. Phys. **129**, 121105 (2008).
[13]M. Wang, E.-Q. Chen, S. Yang, and S. May, J. Chem. Phys. **139**, 024703 (2013).
[14]P. Attard, R. Kjellander, D. J. Mitchell, and B. Jönsson, J. Chem. Phys. **89**, 1664 (1988).
[15]P. Attard and G. N. Patey, Phys. Rev. A **43**, 2953 (1991).
[16]A. Moschel and K. D. Usadel, Phys. Rev. B **51**, 16111 (1995).
[17]A. Hucht and K. D. Usadel, Phys. Rev. B **55**, 12309 (1997).
[18]K. De'Bell, A. B. MacIsaac, and J. P. Whitehead, Rev. Mod. Phys. **72**, 225 (2000).
[19]C. Alvarez, M. Mazars, and J.-J. Weis, Phys. Rev. E **77**, 051501 (2008).
[20]P. Attard and D. J. Mitchell, Chem. Phys. Lett. **133**, 347 (1987).
[21]P. Attard, D. J. Mitchell, and B. W. Ninham, Biophys. J. **53**, 457 (1988).
[22]B. Jönsson, P. Attard, and D. J. Mitchell, J. Phys. Chem. **92**, 5001 (1988).
[23]F. Lado, E. Lomba, and J. J. Weis, Phys. Rev. E **58**, 3478 (1998).
[24]F. Lado, Mol. Phys. **107**, 301 (2009).
[25]M. J. Booth, A. G. Schlijper, L. E. Scales, and A. D. J. Haymet, Comput. Phys. Commun. **119**, 122 (1999).
[26]M. Pernice and H. F. Walker, SIAM J. Sci. Stat. Comput. **19**, 302 (1998).
[27]J. J. Weis and D. Levesque, Adv. Polym. Sci. **185**, 163 (2005).
[28]R. A. Trasca and S. H. L. Klapp, J. Chem. Phys. **129**, 084702 (2008).
[29]J.-P. Hansen and I. R. McDonald, *Theory of Simple Liquids*, 3rd ed. (Academic Press, London, 2006).
[30]J. S. Rowlinson, Mol. Phys. **9**, 217 (1965).
[31]F. Lado, J. Chem. Phys. **47**, 4828 (1967).
[32]F. Lado, J. Chem. Phys. **49**, 3092 (1968).
[33]Y. Rosenfeld and N. W. Ashcroft, Phys. Rev. A **20**, 1208 (1979).
[34]W. H. Press, S. A. Teukolsky, W. T. Vetterling, and B. P. Flannery, *Numerical Recipes: The Art of Scientific Computing*, 3rd ed. (Cambridge University Press, New York, NY, 2007).
[35]W. H. Press and S. A. Teukolsky, Comput. Phys. **4**, 423 (1990).
[36]L. Belloni and I. Chikina, Mol. Phys. **112**, 1246 (2014).
[37]N. Hoffmann, C. N. Likos, and H. Löwen, Mol. Phys. **105**, 1849 (2007).
[38]J. J. Weis, J. Phys.: Condens. Matter **15**, S1471 (2003).
[39]F. Lado, J. Comput. Phys. **8**, 417 (1971).
[40]L. Yu, M. Huang, M. Chen, W. Chen, W. Huang, and Z. Zhu, Opt. Lett. **23**, 409 (1998).
[41]M. Guizar-Sicairos and J. C. Gutierrez-Vega, J. Opt. Soc. Am. A. **21**, 53 (2004).
[42]M. D. Rawn, SIAM J. Appl. Math. **49**, 638 (1989).
[43]K. I. Kou, T. Qian, and F. Sommen, Adv. Appl. Clifford Algebras **17**, 519 (2007).